# Appendices

## A Radius Size, $R$

To approximate Equation 2, we generate controls on a disc (Section 2.2). By using this approximation method, we therefore assume that the probability density function of a step ending at $y$ given that it started at $x$ over the area of the disc, is

$$f(y|x) = \begin{cases} \text{Eq. 2} & \text{if } l_{xy} \leq R \\ 0 & \text{if } l_{xy} > R \end{cases} \tag{1}$$

Therefore, for this approximation to be accurate, the disc needs to be large enough so that the probability of a step longer than $R$ is very small (Figure S1). If we define the radius as $R = l_m \times \gamma$, where $l_m$ is the maximum observed step length, the approximation will improve as $\gamma$ increases. However, as the size of the disc becomes larger, so does the number of controls needed for the approximation. There is no straightforward way to assess this trade-off (i.e., the optimal size of $R$), but we can use importance sampling, based on where we expect the ESF to take large values. We explore the effect of the size of $R$ on the approximation using simulated data, as well as comparing individual polar bear estimates approximated with different values of $\gamma$.

**Simulated Data** We simulated 250 movement tracks $\{x_1, x_2, \ldots, x_n\}$ of length $n = 250$, as described in Section B. For each step, we generated 50 controls on a disc with a radius of the size $R = l_m \times \gamma$, where $\gamma = 0.5, 1.1, 2$. We fit the ESF for each movement track. As expected, $\beta_2$ was estimated with the lowest precision with the smallest radius ($\gamma = 0.5$). It was estimated correctly when $\gamma \geq 1.1$ (Figure S2). However, this represents a simplistic example, where the costs are *only* dependent on step length and $\beta_2 = 15$ is fairly strong selection against costs (i.e., the step length distribution should quickly decay to 0).

**Real Data** We checked the effect of radius size on our polar bear telemetry data. We generated controls on a disc with $R_1 = 1.1 \times l_m$ and $R_2 = 2 \times l_m$ for each individual, fit the models separately, and then compared parameter estimates. Estimates varied up to $\pm 0.15$ for $\beta_2$ (Figure S3), but followed the same general pattern. There was no evidence of systematic bias (i.e., underestimation or overestimation), and variation may be explained by the random generation of controls (which varied between the two trials). $\beta_1$ also varied between the two radius sizes, but this is likely attributable to high uncertainty in the estimates

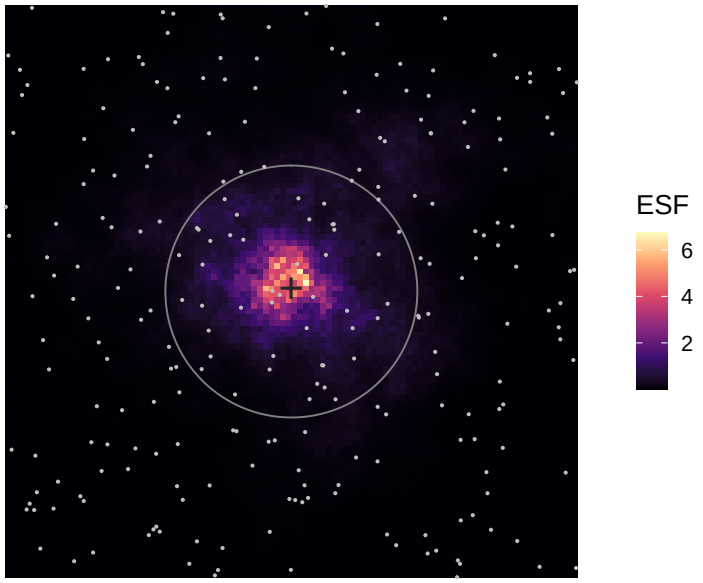


Figure S1: Plot illustrating importance sampling in the ESF. Theoretically, we should sample uniformly over the entire study area (white dots). However, the ESF should decay with distance from the start point (+), due to the effect of step length on costs, and controls generated outside the disc will contribute very little to the approximation (i.e., their ESF is nearly zero). Therefore, for computational convenience, we can just sample within the disc, as long as the radius is large enough.

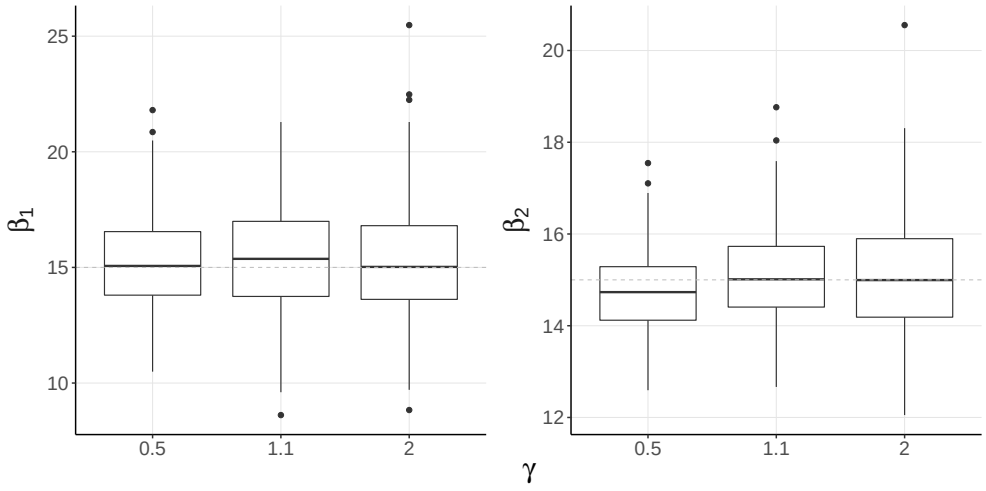


Figure S2: Estimates of $\beta_1$ and $\beta_2$ with $R = \gamma \times l_m$, where $l_m$ is the maximum observed step length and $\gamma = 0.5, 1.1, 2$. Dashed line represents the true parameter value.

(i.e., no clear selection for gains).

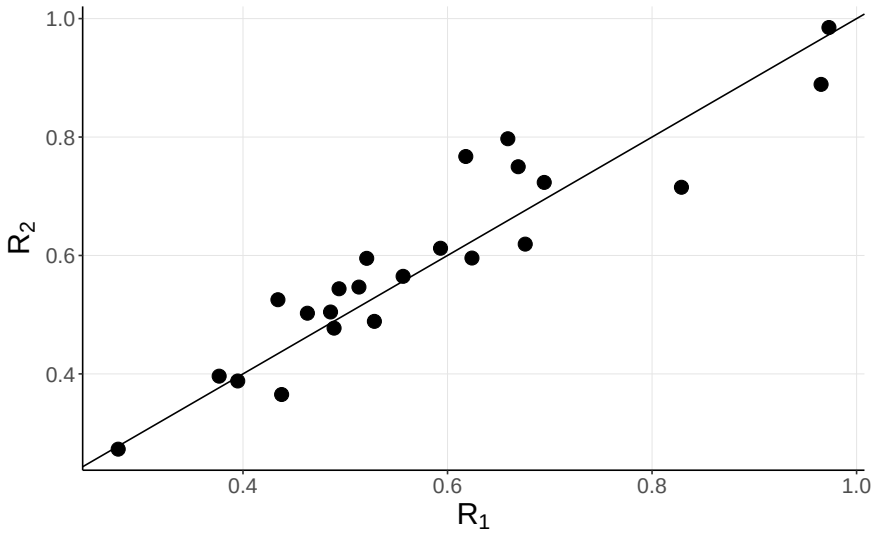


Figure S3: Individual estimates of $\beta_2$ with $R_1 = 1.1 \times l_m$ and $R_2 = 2.0 \times l_m$. Each point is an individual polar bear and the straight line represents a 1:1 relationship.

## B Simulation Study

We ran simulations to assess the performance of the ESF inference method (section 2.2). The main objective was to recover model parameters from movement tracks simulated directly from the ESF, with known parameter values. For all simulations, $G$ was defined as a random covariate field and $C$ was calculated as the step length, both from $[0, 1]$ and assumed to be in the same units.

**Algorithm** We generated $n$ locations $x_1, x_2, \ldots, x_n$, with $x_1$ selected randomly from the study area $\Omega$. For each iteration $i = 1, \ldots, n-1$, we followed these steps to generate $x_{i+1}$:

1. Simulate possible endpoints $\{z_1, z_2, \ldots, z_K\}$ uniformly on a disc centred on $x_i$, with a radius $R = 1$.

2. Evaluate $G$ and $C$ at each endpoint.

3. For $k \in 1, 2, ...K$, sample $x_{i+1}$ from $\{z_1, z_2, \ldots, z_K\}$, with probabilities defined by

$$p_k = \frac{w(x_i, z_k)}{\sum_{j=1}^{K} w(x_i, z_j)}, \tag{2}$$

where $w$ is the ESF (equation 3 in Section 2.1).

**Scenarios** First, we assessed whether the selection strength affected our ability to estimate the parameters, and subsequently, whether certain foraging strategies may be harder to identify. For both $\beta_1$ and $\beta_2$, we considered 15 as a high parameter value. We considered low parameter values to be 0 for $\beta_1$ (no selection for gains), and 5 for $\beta_2$ (very weak selection against costs). We could not use 0 for $\beta_2$, as the ESF simulation algorithm would artificiality constrain the step length through the radius model. We tested different values of $\beta_2$ and found that 5 was the lowest parameter value where the size of the radius no longer affected the simulated step lengths. We combined these parameter values to represent the following movement patterns: i) optimal movement (high values of both parameters), ii) intake maximization (high $\beta_1$, low $\beta_2$), iii) cost minimization (low $\beta_1$, high $\beta_2$), and iv) movement nearly free of energetic considerations (low values of both parameters). Next, we altered the level of spatial autocorrelation in $G$. We simulated the study area $\Omega$ as a $1000 \times 1000$ raster with a resolution of 0.25, and assigned each grid cell a random value [$\sim U(0, 1)$]. We calculated the covariate field for $G$ by using a circular moving average window with diameter $\rho$ (measured in grid units) to control the degree of spatial autocorrelation (Avgar *et al.*, 2016; Michelot, 2019). We created random rasters of $G$ with $\rho = 1, 5, 10, 25$ to reflect four levels of spatially autocorrelated habitat. For each of the 16 scenarios (parameter sets and spatial autocorrelation), we generated 250 movement tracks $\{x_1, x_2, \ldots, x_n\}$ of length $n = 250$. For each track, we tested the inference method using 20 and 200 control locations in the Monte Carlo integration procedure (Section 2.2). All parameters were estimated using MLE.

**Results** In most cases, the parameters were estimated accurately, although $\beta_2$ was generally estimated more precisely than $\beta_1$ (Figure S4). The median (min, max) difference between estimated and known parameter values was $-0.04$ ($-65$, 27) for $\beta_1$ and 0.04 ($-4.8$, 4.7) for $\beta_2$. Spatial autocorrelation in $G$ had a noticeable effect on the precision of $\beta_1$ estimates, but not $\beta_2$. When $\beta_1$ was high, there was a pattern of decreased precision with increased autocorrelation. When $\beta_1$ was low, precision was lowest when spatial autocorrelation was very low ($\rho = 1$) and very high ($\rho = 50$). Spatial autocorrelation is a documented issue in resource selection analyses, which can lead to biased parameter estimates (Northrup *et al.*, 2013). In SSFs and ESFs, high spatial autocorrelation decreases the range of the covariate space that may be explored for each movement step, which may decrease the ability to infer selection, particularly when the number of control locations is low (Northrup *et al.*, 2013). However, in our simulations, the number of control locations used in Monte Carlo integration had negligible effects on the precision or accuracy of parameter estimations. Therefore, in most cases, 20 control locations should be adequate to approximate the likelihood, although we still recommend caution when working with highly spatially autocorrelated environmental covariates.

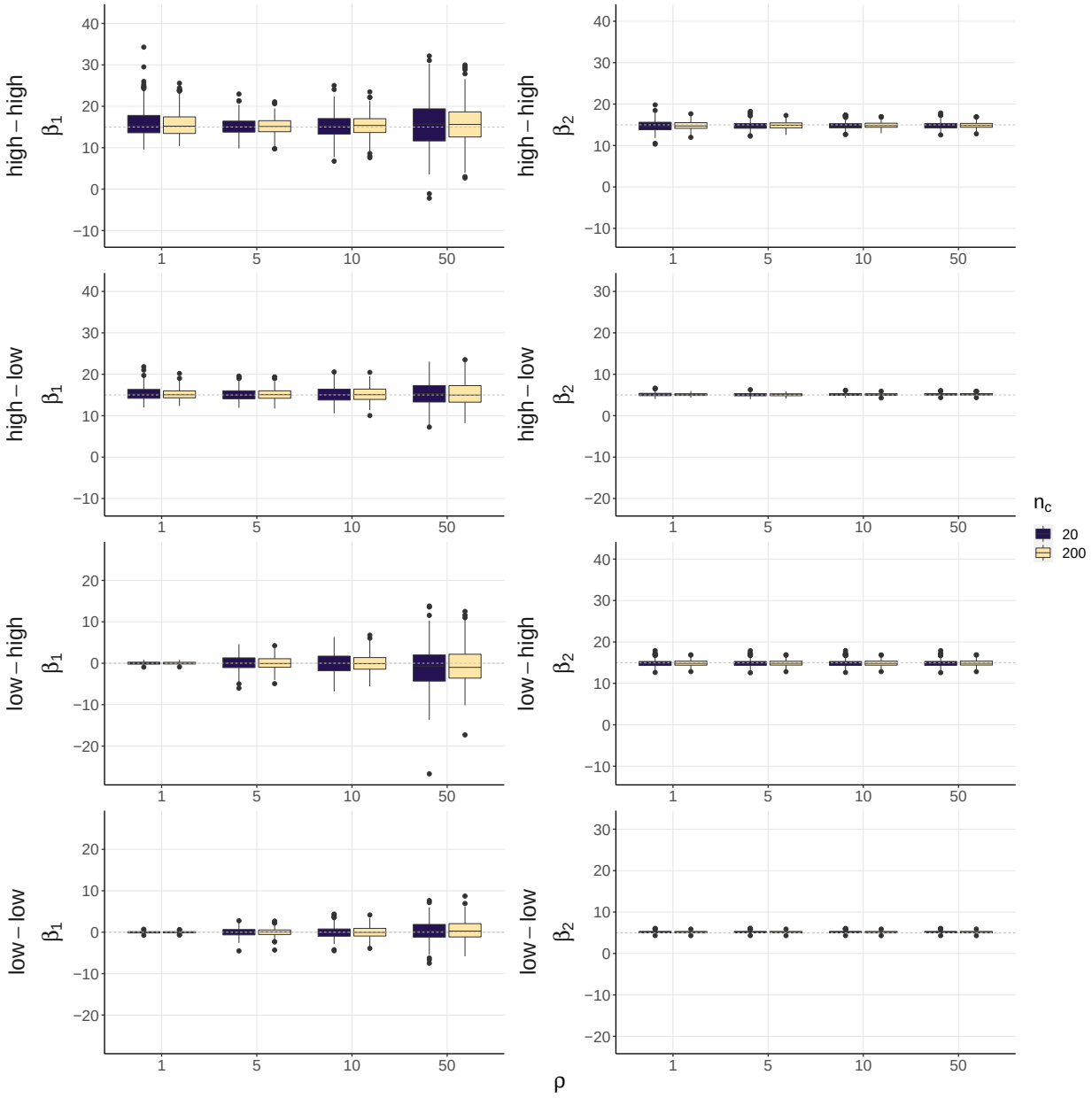


Figure S4: Parameter estimates from the simulations, under 32 different scenarios. Tracks were simulated either of four sets of parameters: "high-high" ($\beta_1 = 15$, $\beta_2 = 15$), "high-low" ($\beta_1 = 15$, $\beta_2 = 5$), "low-high" ($\beta_1 = 0$, $\beta_2 = 15$), and "low-low" ($\beta_1 = 0$, $\beta_2 = 5$). $\rho$ refers to the level of spatial autocorrelation in the energetic gain covariate $G$, and $n_c$ is the number of controls used in Monte Carlo integration. Dashed line is the true parameter value.

## C Defining Energetic Covariates

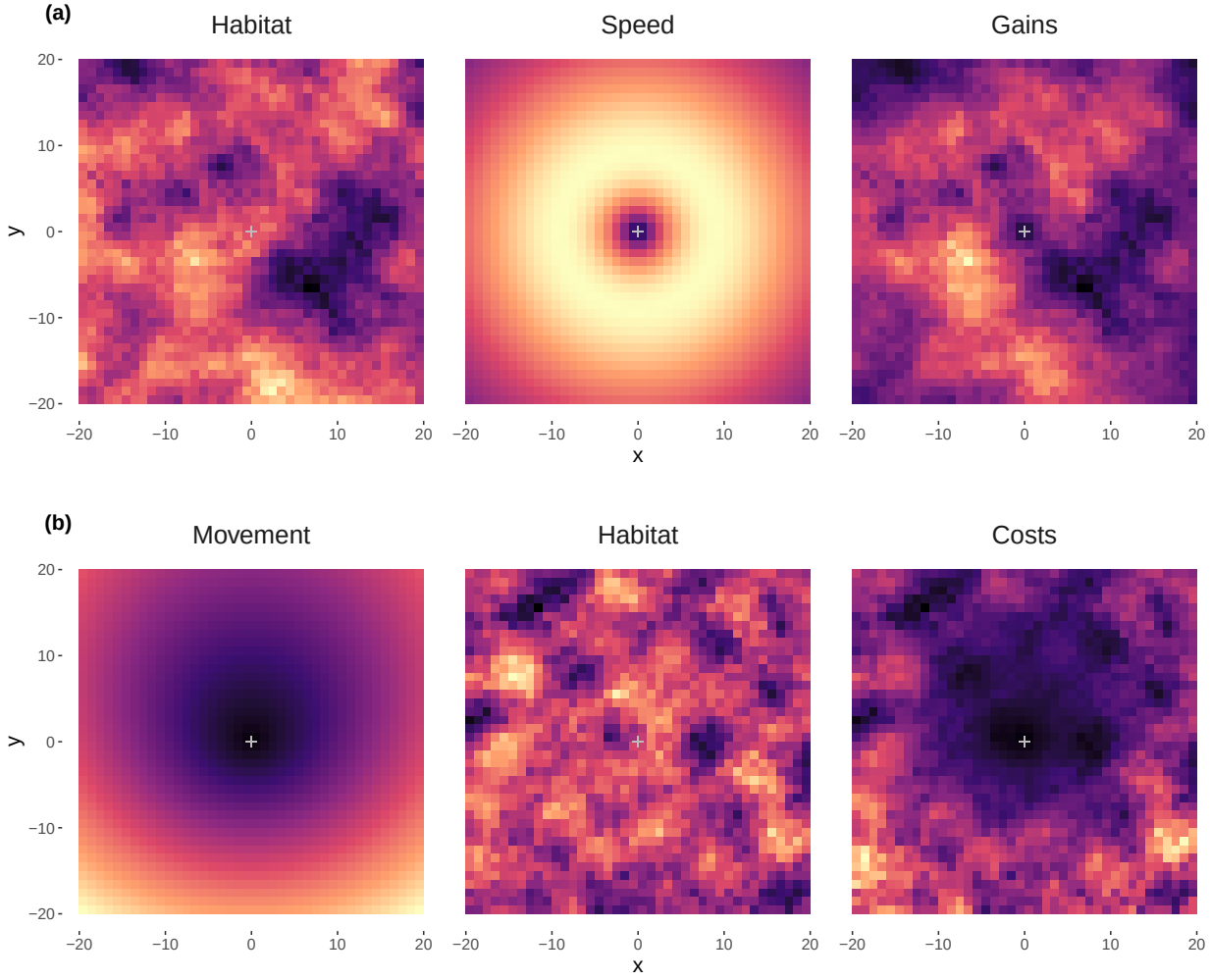


Figure S5: Example energetic gain $G$ (a) and energetic cost $C$ (b) formulations. In all panels, higher values are lighter in colour. In both (a) and (b), the third panel is a product of the first two panels, which represent movement and habitat components. In (a), energetic gains are composed of an energetically beneficial habitat covariate (e.g., forage biomass) scaled to the speed travelled. In this case, the effect of movement speed is gamma distributed ($k = 2$, $\theta = 2.2$) about the start point to represent decreased foraging potential at low and high speeds. In (b) the energetic costs are defined by the distance and turning angle from the start point (+; assuming movement up the y-axis), combined with a habitat covariate in which higher values increase energy expenditure.

# D Case Study

## D.1 Study Area and Field Sampling

Field sampling was done in Beaufort Sea, Canada (Figure S6). Sea ice in the area is mostly annual, with a flaw lead that separates near-shore areas of stable landfast ice and off-shore drifting pack ice (Carmack & Macdonald, 2002). The lead widens in spring and forms an active sea ice zone with high productivity (Pilfold *et al.*, 2014), before most ice disappears by mid-summer (Stern & Laidre, 2016). Sea ice drift is characterized by the clockwise Beaufort Gyre, which is strengthening with climate change (Hutchings & Rigor, 2012; Petty *et al.*, 2016), and increasing the energetic expenditure of polar bears in the area (Durner *et al.*, 2017).

Following standard capture procedures (Stirling *et al.*, 1989), polar bears were sighted and immobilized in April-May of 2007-2011. Bears were fitted with GPS collars (Telonics, Mesa, AZ) set to a collect locations at a 4-hour resolution (relayed via the Argos satellite system; CLS America, Lanham, MD), and programmed to release after 1-2 years. The age of each bear was determined by analysing cementum growth layers of an extracted vestigial premolar (Calvert & Ramsay, 1998), and sex was determined in the field. Capture and handling was approved by the University of Alberta BioSciences Animal Care and Use Committee following guidelines from the Canadian Council on Animal Care.

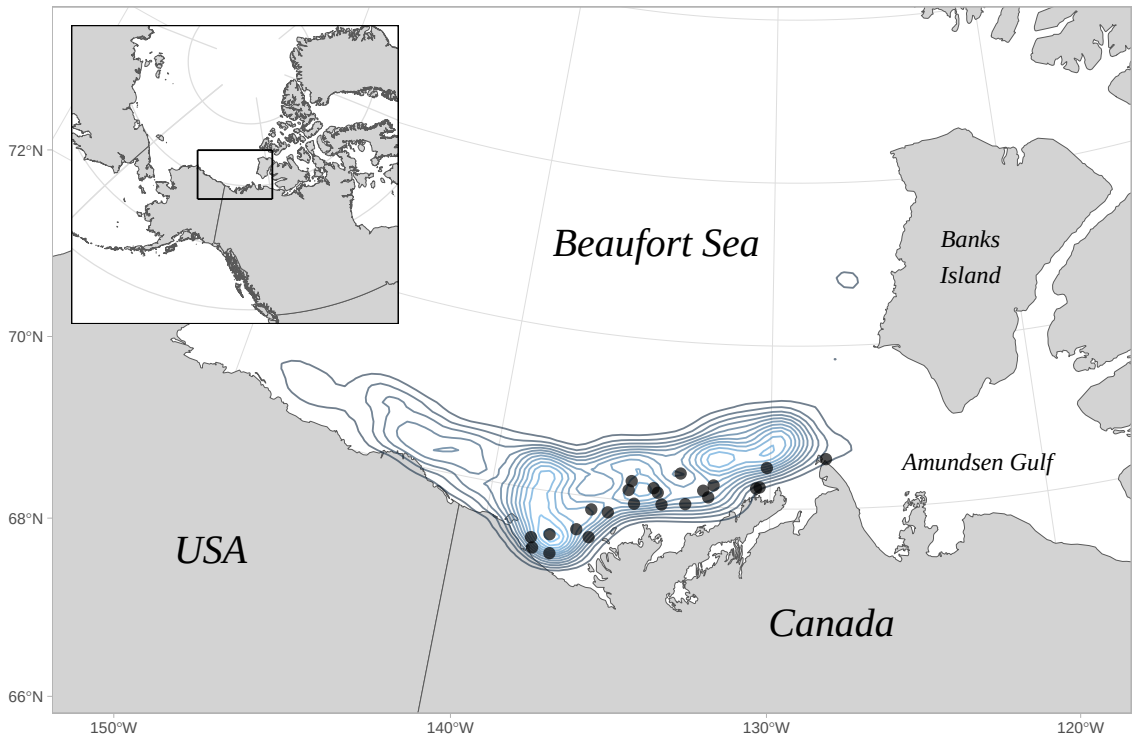


Figure S6: Study area in the Beaufort Sea, Canada. Circle points are polar bear collar deployment locations, and contour lines show the density of satellite telemetry data for all individuals (once regularised and limited to the spatiotemporal extent of the energetic gains raster).

### D.2 Polar Bear Cost Modelling

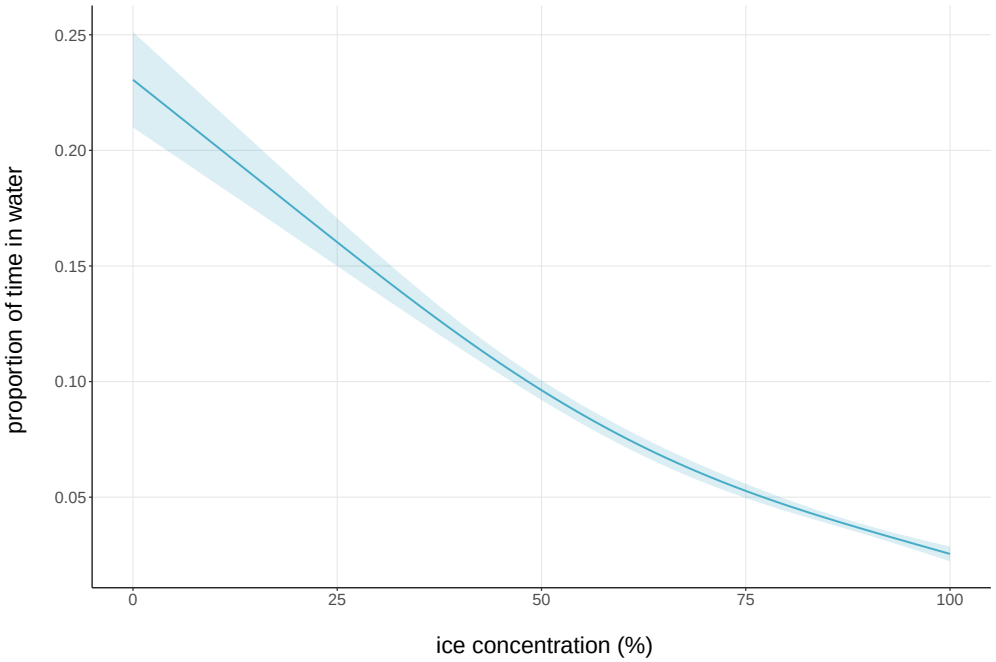


Figure S7: Estimated proportion of time spent in water relative to ice concentration, modelled with a generalized additive model (GAM). Data from Lone *et al.* (2018). Shaded area represents the standard error of the model fit.

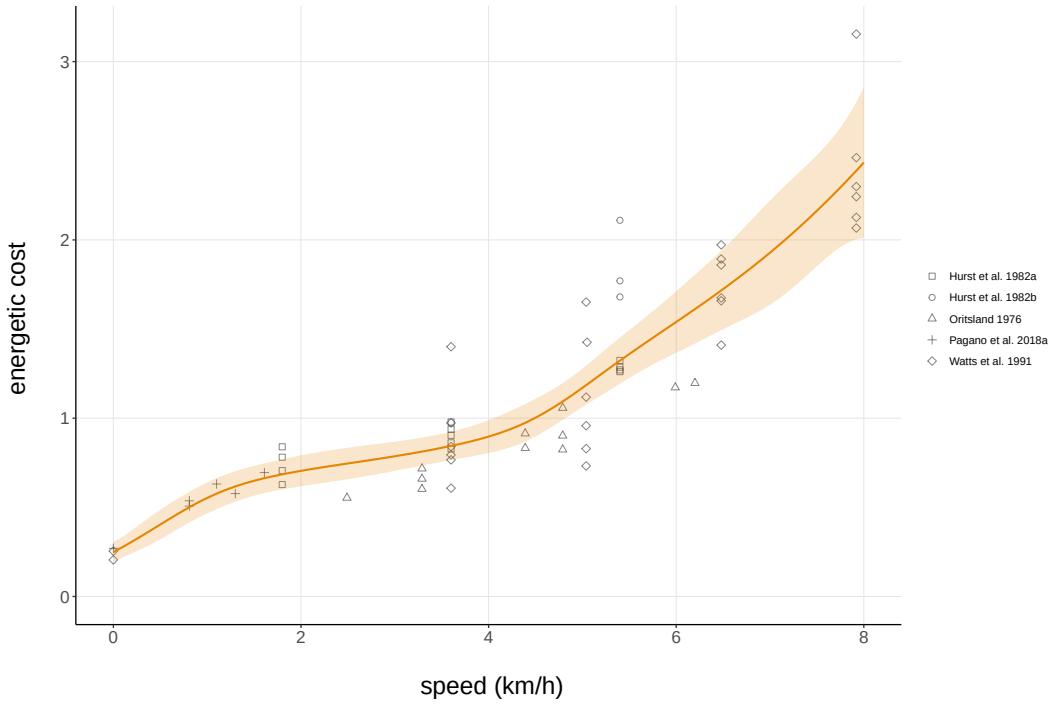


Figure S8: Relationship between polar bear walking speed (km/h) and energy expenditure (oxygen consumption; mL O2/g/hr) from six reference studies. Solid line is the predicted relationship from a monotonically constrained generalized additive model (gamma distribution, logit link function). Shaded area represents the standard error of the model fit.

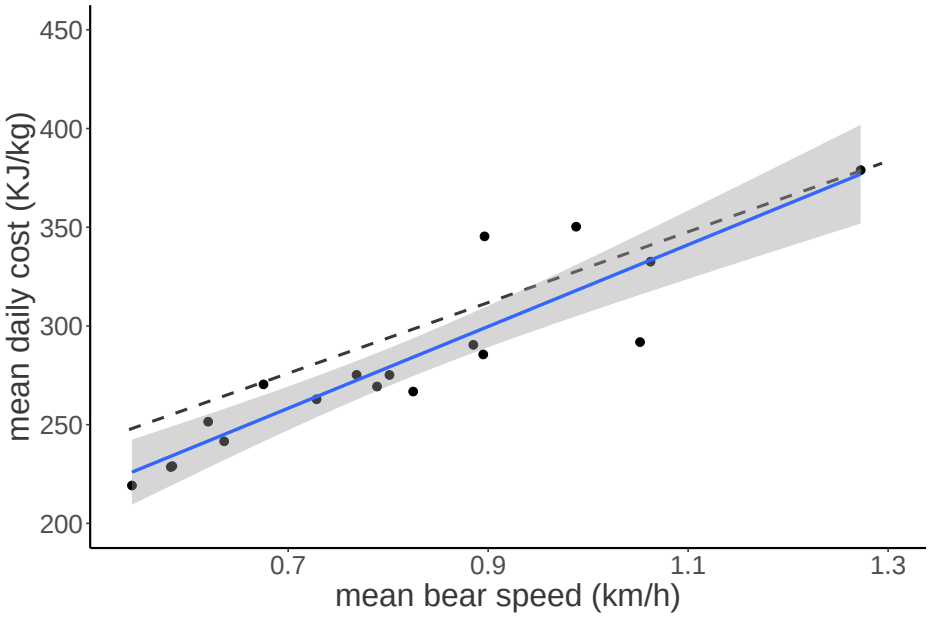


Figure S9: Relationship between mean daily movement speed (km/h) and daily energy expenditure (kJ/kg) for individuals with more than 25 days of locations with 6 locations (blue line) compared to the estimated relationship from doubly-labelled water (Pagano & Williams, 2019).

# References


Avgar, T., Potts, J. R., Lewis, M. A. & Boyce, M. S. (2016). Integrated step selection analysis: bridging the gap between resource selection and animal movement. *Methods in Ecology and Evolution*, 7, 619–630.

Calvert, W. & Ramsay, M. A. (1998). Evaluation of Age Determination of Polar Bears by Counts of Cementum Growth Layer Groups. *Ursus*, 10, 449–453.

Carmack, E. C. & Macdonald, R. W. (2002). Oceanography of the Canadian shelf of the Beaufort Sea: A setting for marine life. *Arctic*, 55, 29–45.

Durner, G. M., Douglas, D. C., Albeke, S. E., Whiteman, J. P., Amstrup, S. C., Richardson, E. S., Wilson, R. R. & Ben-David, M. (2017). Increased Arctic sea ice drift alters adult female polar bear movements and energetics. *Global Change Biology*, 23, 3460–3473.

Hutchings, J. K. & Rigor, I. G. (2012). Role of ice dynamics in anomalous ice conditions in the Beaufort Sea during. *Journal of Geophysical Research*, 117, C00E04.

Lone, K., Kovacs, K. M., Lydersen, C., Fedak, M., Andersen, M., Lovell, P. & Aars, J. (2018). Aquatic behaviour of polar bears (Ursus maritimus) in an increasingly ice-free Arctic. *Scientific Reports*, 8, 9677.

Michelot, T. (2019). *Stochastic models of animal movement and habitat selection*. Ph.D. thesis.

Northrup, J. M., Hooten, M. B., Anderson, C. R. J. & Wittemyer, G. (2013). Practical guidance on characterizing availability in resource selection functions under a use-availability design. *Ecology*, 94, 1456–1463.

Pagano, A. M. & Williams, T. M. (2019). Estimating the energy expenditure of free-ranging polar bears using tri-axial accelerometers: A validation with doubly labeled water. *Ecology and Evolution*, 9, 4210–4219.

Petty, A. A., Hutchings, J. K., Richter-Menge, J. A. & Tschudi, M. A. (2016). Sea ice circulation around the Beaufort Gyre: The changing role of wind forcing and the sea ice state. *Journal of Geophysical Research: Oceans*, 121, 3278–3296.

Pilfold, N. W., Derocher, A. E. & Richardson, E. S. (2014). Influence of intraspecific competition on the distribution of a wide-ranging, non-territorial carnivore. *Global Ecology and Biogeography*, 23, 425–435.

Stern, H. L. & Laidre, K. L. (2016). Sea-ice indicators of polar bear habitat. *Cryosphere*, 10, 2027–2041.

Stirling, I., Spencer, C. & Andriashek, D. S. (1989). Immobilization of polar bears (Ursus maritimus) with Telazol in the Canadian Arctic. *Journal of Wildlife Diseases*, 25, 159–168.